SAND2013-9340C

Comparison of Multiple Mass Property Estimation Techniques on SWiFT Vestas V27 Wind Turbine Nacelles and Hubs

Timothy Marinone, David Cloutier, and Kevin Napolitano
ATA Engineering, San Diego, CA, 92130

Bruce LeBlanc
Sandia National Laboratories,[1] Albuquerque, NM, 87185

ABSTRACT

Rigid body mass properties have proven to be valuable data for use in a variety of analyses; a complex structure can be simplified into a single mass element provided the mass, CG, and moments of inertia are known. Because traditional experimental methods often require significant time, effort, and resources to set up and perform, much work has been done to find ways to use data from other test setups to obtain these properties.

In this paper, multiple methods used to obtain rigid body mass properties were performed on two different test articles: a Vestas V27 wind turbine hub and a Vestas V27 wind turbine nacelle. The methods compared are use of a load cell and bifilar pendulum, use of mass-line values obtained from measured transfer functions, and use of modal parameters extracted from rigid body modes. The modal parameter method produced the most accurate results, while the mass-line approach was nearly as accurate but suffered from some experimental error.

INTRODUCTION

Sandia National Laboratories (SNL) is developing the Scaled Wind Farm Technology (SWiFT) center to enable rapid, cost-efficient testing and development of transformative wind energy technology. The site is intended to study complex turbine wake interactions and focus on damage mitigation, improved power performance, and recommended future site layouts. Since this site is designed to be open source and to provide data to all interested parties, the models must be accurate enough to be used for the desired analyses while preserving Vestas' proprietary information. For this paper, the hub and nacelle of the Vestas V27 (V27) wind turbines used on site were tested to obtain the mass inertia properties, as this allows the model to accurately reflect the wind turbines installed while eliminating the need to fully model the hub and nacelle.

The traditional approach to obtaining inertia properties, commonly taught as part of an undergraduate course sequence, uses a bifilar or trifilar pendulum procedure. If the test article is unwieldy or complex, however, this approach often requires a complex fixture design to be used. In addition, large experimental errors are introduced if assumptions inherent in the procedure are not satisfied.

Two methods for obtaining inertia properties from modal data using mass-line values or using modal parameters extracted from rigid body modes were presented by Bretl and Conti [1]. In their paper, they presented the mathematical framework for both techniques and used them to obtain the rigid body mass properties of an engine assembly supported by elastomeric mounts to the ground. Values obtained by the two methods were consistent and indicated the usefulness of the techniques. These and other techniques have been used for other test articles [2–6] and have generally produced good results.

REVIEW OF MASS INERTIA MATRIX

The matrix form of the equation of motion for a rigid body is written as

---

[1] Sandia is a multiprogram laboratory operated by Sandia Corporation, a Lockheed Martin Company, for the U.S. Department of Energy under Contract DE-AC04-94AL85000.

$$\begin{Bmatrix} F_x \\ F_y \\ F_z \\ M_x \\ M_y \\ M_z \end{Bmatrix} = \begin{bmatrix} m & 0 & 0 & 0 & 0 & 0 \\ 0 & m & 0 & 0 & 0 & 0 \\ 0 & 0 & m & 0 & 0 & 0 \\ 0 & 0 & 0 & I_{xx} & -I_{xy} & -I_{xz} \\ 0 & 0 & 0 & -I_{xy} & I_{yy} & -I_{yz} \\ 0 & 0 & 0 & -I_{xz} & -I_{yz} & I_{zz} \end{bmatrix} \begin{Bmatrix} a_x \\ a_y \\ a_z \\ \alpha_x \\ \alpha_y \\ \alpha_z \end{Bmatrix}. \qquad \text{Equation 1}$$

Provided that the forces F_x, F_y, F_Z and moments M_x, M_y, M_Z input into the test article are known, and the output linear and angular accelerations $a_x, a_y, a_Z, \alpha_x, \alpha_y, \alpha_Z$ are measured, the inertia measurements can easily be obtained. Although this condition can be reasonably represented by testing the structure in an approximately free-free boundary condition with soft supports, the common setup for modal testing does not involve measuring the moments imparted to the system, the linear acceleration at the CG location, or the angular acceleration experienced by the test article. As a result, the approaches used are rewritten to account for the use of multiple accelerometers measuring only linear accelerations.

For all of the following approaches, the rigid body transformation matrix R is used, which maps the six DOF of the origin to the six DOF of each test node.

MASS-LINE APPROACH—VARIATION A

The equation for the mass-line approach is valid at frequencies above the rigid body modal frequencies and well below the flexible body frequencies of the test article. In this range, the assumption that the structure is moving as a rigid body still holds, and the values of all the FRFs are constant as a function of frequency.

The moments and acceleration of the CG can be written and substituted into Equation (1) and rearranged so that CG locations and mass moments of inertias are the unknowns. The resulting equation is

$$\begin{Bmatrix} F_x - ma_{ox} \\ F_y - ma_{oy} \\ F_z - ma_{oz} \\ YF_z - ZF_y \\ ZF_x - XF_z \\ XF_y - YF_x \end{Bmatrix} = \begin{bmatrix} 0 & -m\alpha_z & m\alpha_y & 0 & 0 & 0 & 0 & 0 & 0 \\ m\alpha_z & 0 & -m\alpha_x & 0 & 0 & 0 & 0 & 0 & 0 \\ -m\alpha_y & -m\alpha_x & 0 & 0 & 0 & 0 & 0 & 0 & 0 \\ 0 & F_z & -F_y & \alpha_x & 0 & 0 & -\alpha_y & 0 & -\alpha_z \\ -F_z & 0 & F_x & 0 & \alpha_y & 0 & -\alpha_x & -\alpha_z & 0 \\ F_y & -F_x & 0 & 0 & 0 & \alpha_z & 0 & -\alpha_y & -\alpha_x \end{bmatrix} \begin{Bmatrix} x_{cg} \\ y_{cg} \\ z_{cg} \\ I_{xx} \\ I_{yy} \\ I_{zz} \\ I_{xy} \\ I_{yz} \\ I_{xz} \end{Bmatrix}. \qquad \text{Equation 2}$$

Fx, Fy, and Fz are the components of the force vector in the “x,” “y,” and “z” directions, and X, Y, and Z are distances of the applied load to the origin. It is assumed that the mass of the test article has also been measured. The left-hand side and the matrix on the right-hand side are known and measured quantities. The vector containing the CG locations and the inertia terms is unknown. Test data from different frequencies and different forcing locations can be added to the forcing vector and the matrix, and then the CG and inertia terms can be solved for in a least-squares sense.

MASS-LINE APPROACH—VARIATION B

An alternative variation using mass-line values can be formulated where the mass of the object has not been measured. The fully populated FRF matrix is transformed from physical degrees of freedom to rigid body degrees of freedom by the rigid body transformation matrix. The rigid body FRF matrix can then be evaluated over the mass-line frequency range and used to calculate the rigid body mass matrix as shown. Then the rigid body mass matrix can be rearranged to yield the familiar terms of mass, CG, and moments of inertia.

$$H_{RBM} = R^{*} H \ . \qquad \text{Equation 3}$$

$$MRB = \left[\left(R^{T} R\right)^{-1} R^{T}\right] H_{RBM} \left[\left(R^{T} R\right)^{-1} R^{T}\right]. \qquad \text{Equation 4}$$

RIGID BODY MODAL PARAMETER ESTIMATION APPROACH

Test-measured rigid body mode shapes can also be used to estimate the rigid body mass properties. The assumption in this method is that rigid body mode shapes are, in fact, rigid and not contaminated by the flexible mode shapes. The fully populated mass matrix can be obtained from the rigid body shapes as shown. The rigid body mass matrix can then be calculated by premultiplying by the rigid body transformation matrix; then the rigid body mass matrix can be rearranged to yield the familiar terms of mass, CG, and moments of inertia.

$$M = \left[\left(\Phi^{*T} \Phi^{*}\right)^{-1} \Phi^{*T}\right] \left[\left(\Phi^{T} \Phi\right)^{-1} \Phi^{T}\right]. \qquad \text{Equation 5}$$

$$MRB = R^{-1} * M * R \ . \qquad \text{Equation 6}$$

TEST ARTICLES

Testing was performed on the nacelle and hub of the V27 wind turbines used in SNL's SWiFT facility. The hub was suspended on air bags, and a test-display model was created, as shown in Figure 1. Drive point measurements were obtained through impacts at all nine response DOF to create a fully populated transfer function matrix for use in obtaining the mass lines. Two shakers were also used to excite the hub to ensure highly accurate rigid body modes. The hub was also suspended rigidly to use the bifilar pendulum approach for comparison.

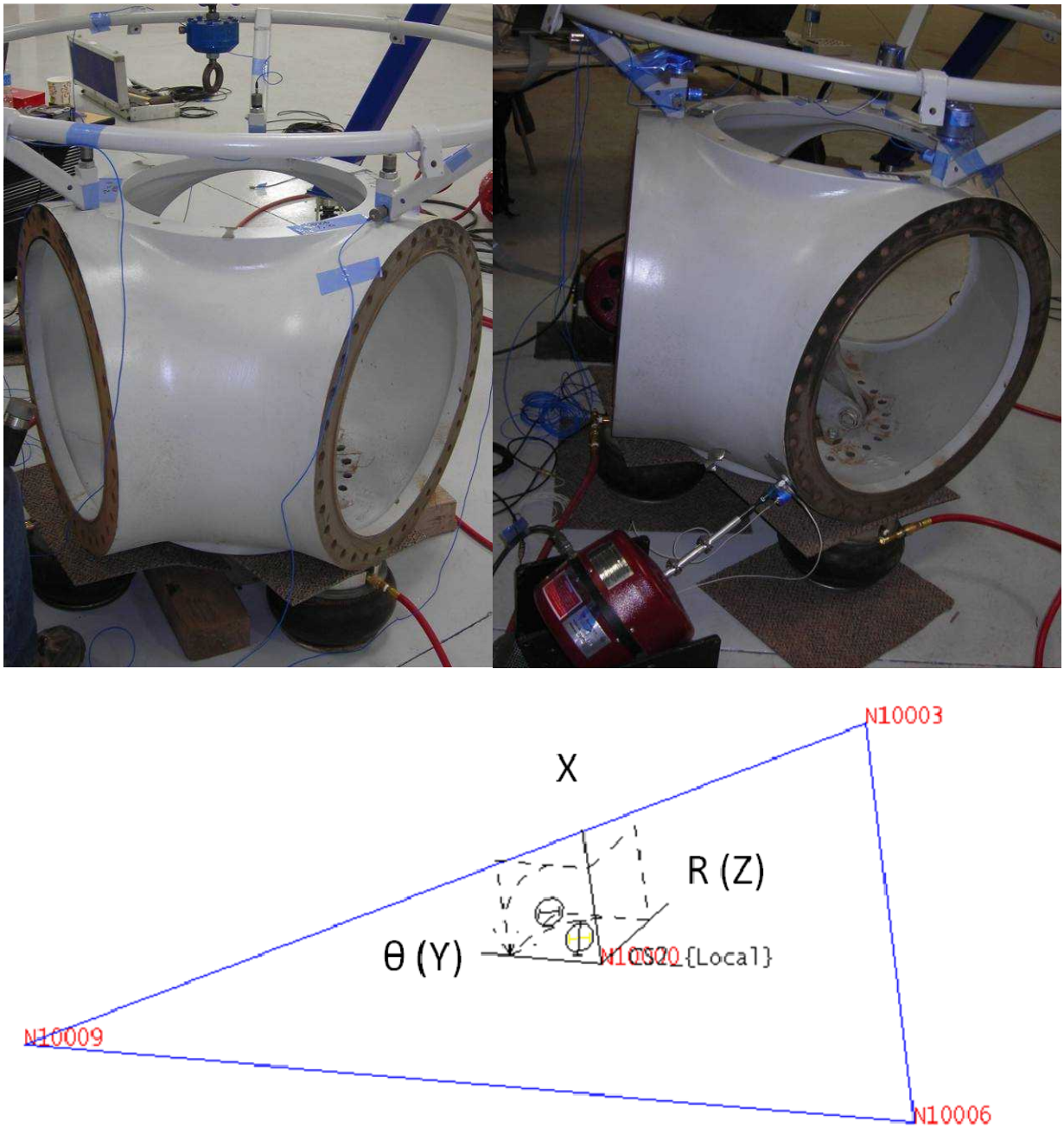

Figure 1. Hub supported (upper left), hub excited by shakers (upper right), and test-display model showing node locations (bottom).

The nacelle was suspended on air bags and a test-display model was created, as shown in Figure 2. Two shakers were also used to excite the nacelle to ensure highly accurate rigid body modes.

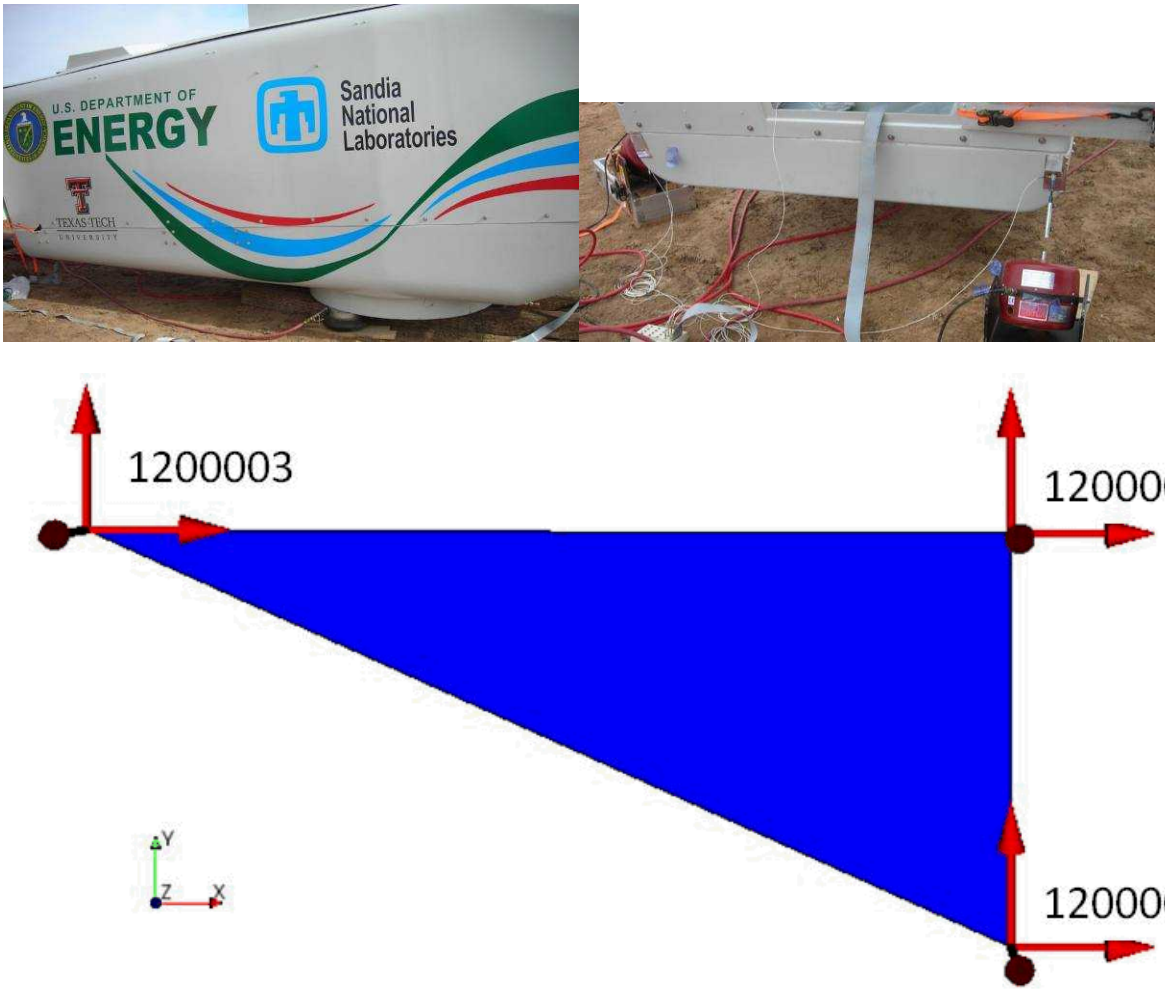

Figure 2. Nacelle supported (upper left), nacelle excited by shakers (upper right), and test-display model showing node locations (bottom).

DATA COLLECTION AND SIGNAL PROCESSING

Seismic accelerometers (PCB 393B04) were mounted to both the hub and nacelle at the node locations in all three axes. Multi-Sine sweeps at 0.2 decades/minute were run with sweeps between 1 and 50 Hz for a total of 730 seconds, while the data was sampled at 128 Hz. This sample rate was sufficient to capture the entire response of the structure while providing sufficient frequency resolution for the modal parameter estimation. Impacts were performed every 32 seconds, and data was sampled at 128 Hz.

Signal processing for the shaker runs used a Hanning broad window with overlap averaging. The impact runs were processed with no window since the excitation and response signals were near zero at the beginning and end of each frame of data.

TEST RESULTS

This section documents the test results. The rigid body modes were estimated for the two nacelles and one hub. The mass-line approach was only applied to the hub.

Figure 3 shows the power spectrum mode-indicator function (PSMIF) for the nacelle with a single reference. While two shakers were used during the test, a single reference provided better fits and mass estimation than both references. The PSMIF, as the summation of all FRFs multiplied by each FRF conjugate, is an ideal function to visualize the overall response of the structure. The six rigid body modes are observed in the six peaks of the response. To evaluate the quality of the rigid body modes obtained, the PSMIF was then synthesized using only the six rigid body modes. The synthesized PSMIF shows a high level of correlation with the test data. As such, there is confidence that the extracted rigid body modes will accurately describe the inertia properties of the nacelles.

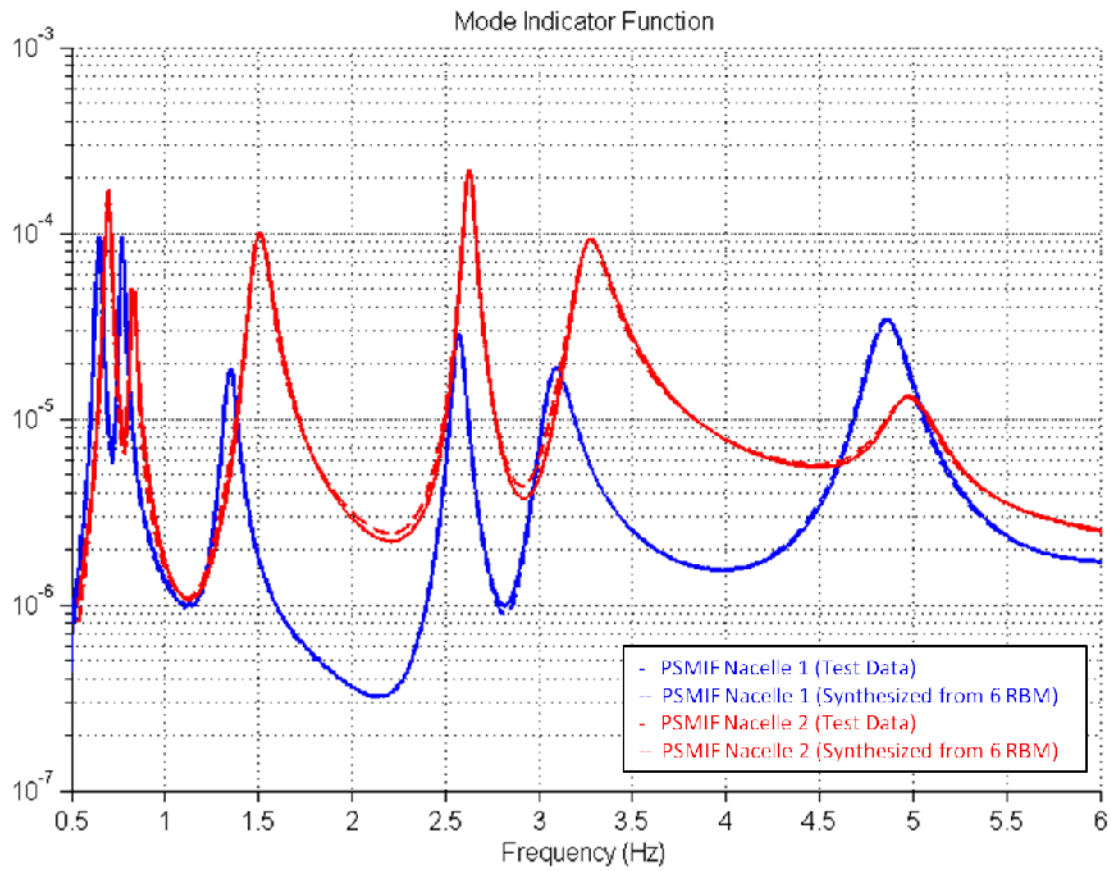

Figure 3. PSMIF for both nacelles comparing test data to synthesized data from the six rigid body modes.

Figure 4 shows the complex mode-indicator function (CMIF) for testing the hub with two shakers. Again, all six rigid body modes can be seen in the peaks of the response (the CMIF is plotted for both shaker references in order to clearly distinguish modes 5 and 6). To evaluate the quality of the rigid body modes obtained, the CMIF was then synthesized using only the six rigid body modes. The synthesized CMIF shows a high level of correlation with the test data. As such, there is confidence that the extracted rigid body modes will accurately describe the inertia properties of the hub as well.

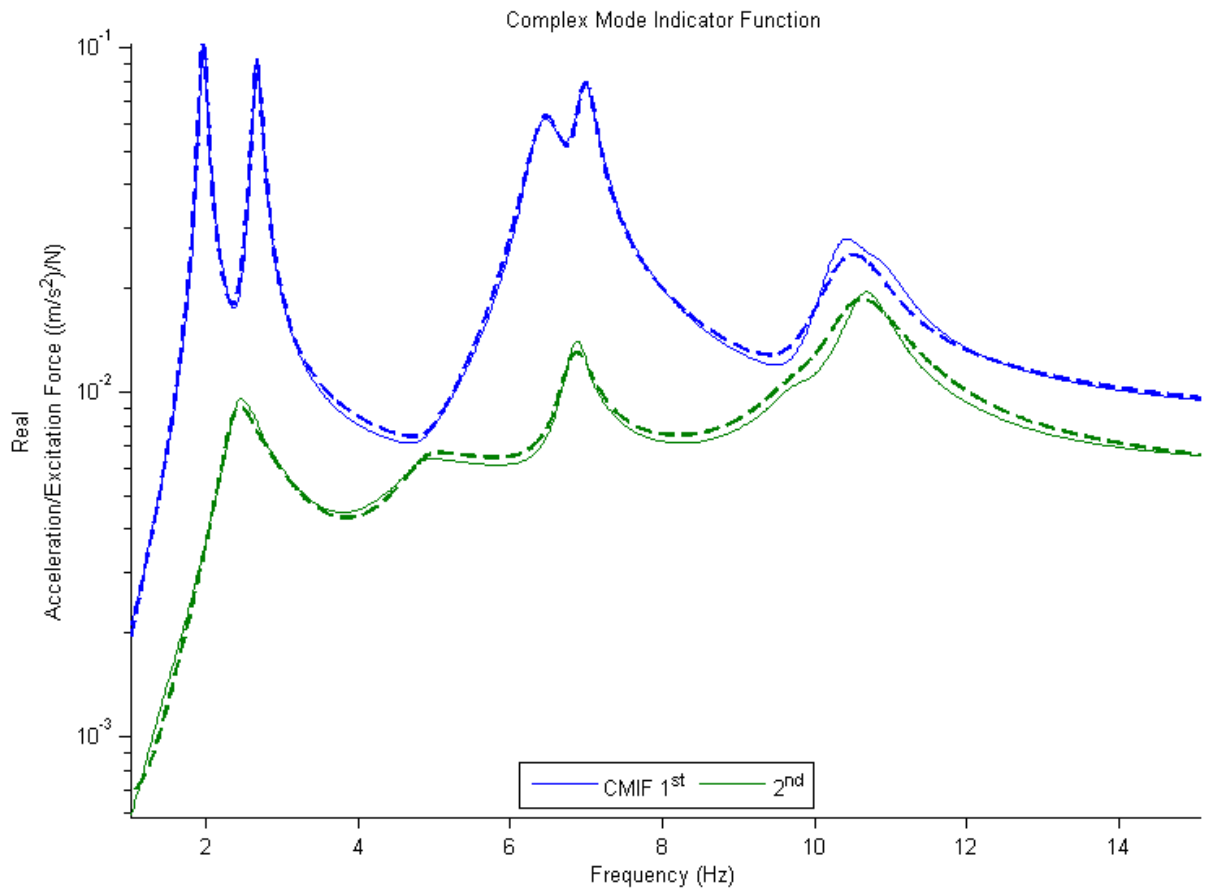

Figure 4. CMIF for the hub comparing test data to synthesized data from the six rigid body modes.

Figure 5 shows the drive point measurements for all of the DOFs where the six rigid body modes are evident in the peaks seen in the responses. There are clear mass lines from 20 to 50 Hz, showing good separation between the rigid body and flexible modes. As seen in the zoomed-in portion, however, there is a small but noticeable oscillation in some of the mass lines, which is associated with experimental error caused by double impacts at some of the less-repeatable drive points. As a result, there is expected to be some error involved in the estimation of the terms using this method.

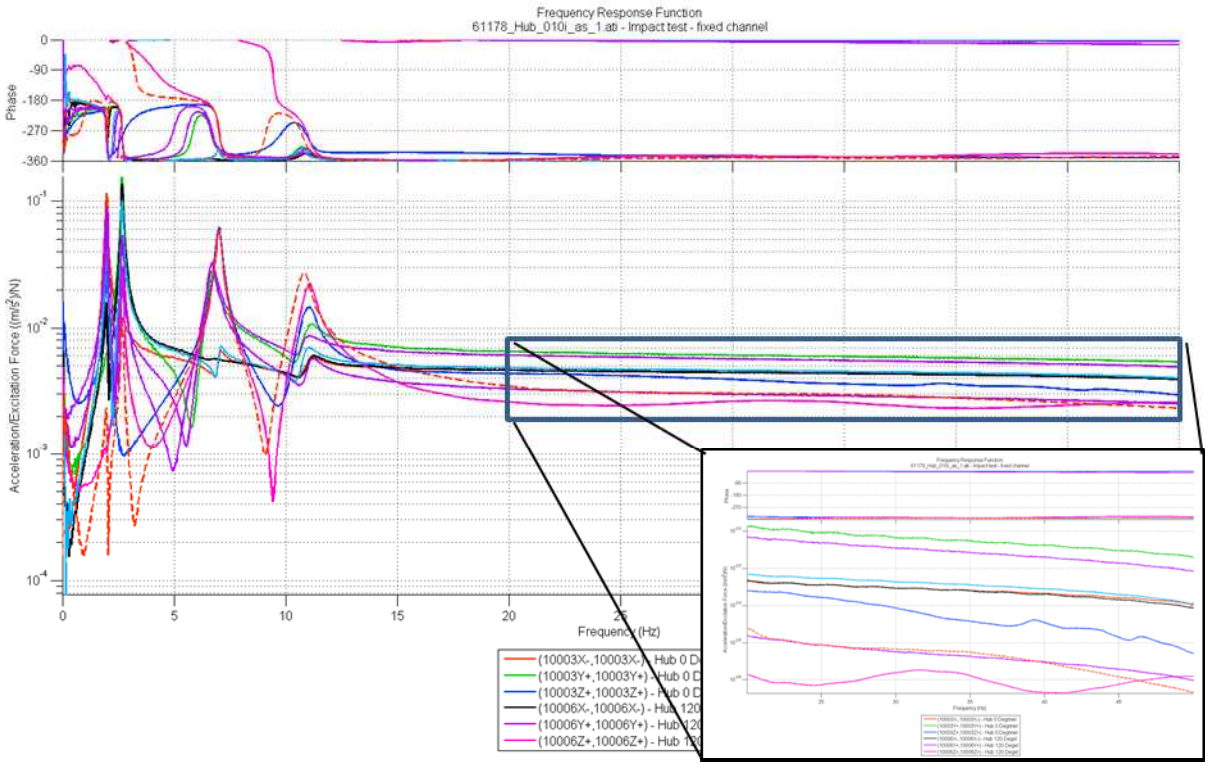

Figure 5. Drive point FRFs from impact runs, showing mass lines.

The inertia results from modal inversion for the nacelle are shown in Table 1. The masses of the nacelles were also measured independently by a crane company during transportation, and these are included for completeness. The mass and CG properties of nacelle 3 were also obtained, but modal testing was not performed on that nacelle.

Table 1. Final list of inertia properties for V27 nacelles.

Mass and Inertia Properties of V27 Nacelles				
Property	**Nacelle #**	**Crane**	**Load Cell**	**Modal Inversion**
Mass (kg)	**1**	6804	7038	5577
	2	6577	6781	5551
	3	6668	7203	
CGx (m)	**1**		0.67	0.25
	2		0.61	0.16
	3		0.65	
CGy (m)	**1**		0.09	0.04
	2		0.07	-0.08
	3		0.09	
CGz (m)	**1**			0.06
	2			0.12
	3			
Ixx (kg*m^2)	**1**			2569
	2			2453
Iyy (kg*m^2)	**1**			9937
	2			10876
Izz (kg*m^2)	**1**			9038
	2			10141

The two nacelles have fairly consistent properties, which were expected due to the assumed similarity in manufacture of the nacelles. The CG of the nacelles in the X direction (fore-aft) is aft of the origin; however, the CG measured in the modal inversion method is closer to the origin than that measured with load cells. The aft CG is expected, as the nacelle should be balanced when the rotor is assembled: without the rotor, the nacelle will be significantly back-heavy. The CG about the Y direction (side-side) is relatively close to the origin, although computed on the opposite side for nacelle 2 using the modal inversion method. The offset is expected to be positive due to the generator being primarily located on the positive-Y side of the nacelle.

Substantial rigging was used when the nacelles were being lifted by the crane, which accounts for some of the discrepancy in the masses obtained between the crane, load cell, and modal inversion methods. Additionally, oil and equipment were installed after the initial inertia testing, changing the mass and CG of the nacelle. The results obtained from the crane and the load cell are assumed to be more accurate than the modal inversion method, as those methods obtained the loads directly from the calibrated load cells, in contrast to estimating them from the modal mass of the rigid body shapes. The error seen using modal inversion may be due to error in measurement, curve-fitting, or accelerometer location measurement. However, the mass and CG are within 20% of the load cell results, which indicates that the moment of inertia terms are reasonably accurate. Finally, the moment of inertia about the Y-axis is the largest, which is expected since the mass is most spread out about the Y-axis.

The modal inversion method and the mass-line inversion method were used to calculate the rigid body mass matrix of the hub. The resulting terms were compared to the mass obtained from the load cell and the inertia term obtained from the bifilar pendulum approach. Table 2 lists the various terms obtained from all of the methods used.

Table 2. Final list of inertia properties for V27

Mass and Inertia Properties of V27 Hubs (Pitch Yaw Linkage Included)					
Property	**Hub #**	**Load Cell**	**Bifilar Pendulum**	**Modal Inversion****	**Mass Line Inversion**
Mass (kg)	**1**	481.7		508.1	483.7
	2	474.0			
CGx (m)*	**1**			-0.438	-0.754
Cgy (m)*				0.015	0.105
CGz (m)*				0.005	-0.143
Ixx (kg*m^2)			26.6	69.1	110.8
Iyy (kg*m^2)				76.3	343.6
Izz (kg*m^2)				86.2	151.6
*** Origin Defined at Front Face of Hub Rotor About the Center Using Rotor Csys**					
**** Includes the Effective Mass of the Airbags**					

As seen in the table, the modal inversion and mass-line inversion methods yield approximately the same mass as the load cell, to within 5%. The CG locations are similar between both methods, but there is an observable discrepancy between the two. The inertia for the bifilar pendulum is significantly lower than either of the two methods, and the mass-line inversion is noticeably higher than the modal inversion.

All four methods used to obtain the mass and inertia properties are discussed here to explain possible sources of error and to comment on their accuracy. The load cell used to measure the mass is a calibrated transducer with accuracy down to the tenth of a kilogram, so these measurements are assumed to be accurate. Use of the bifilar pendulum assumes that the two straps are equal in length and hang perfectly vertical, but since visual inspection of the straps shows that neither of these assumptions was valid, the resulting term is likely to be inaccurate.

The modal inversion was shown to have a high fit between the test data and the synthesized response. The highest percent error on any of the modes was 2%, also indicating a high level of correlation. The result for the mass is high due to the influence of the airbags, as the upper airbag plate is considered part of the system and is therefore added to the weight. The results seen for the CG appear reasonable; the Y and Z terms should be close to zero, as the hub is symmetrical about those two axes. The X term should be about half a meter, as the test origin was obviously away from the expected CG of the hub. The inertia terms about Y and Z are also fairly close, which was expected due to the symmetry of the hub.

The mass-line inversion was shown to have some oscillations, which indicated that the estimated results would therefore contain error. Although the results are fairly reasonable, they are high for all of the CG and inertia terms. Due to the hub's physical structure, drive point measurements of less-than-ideal quality were obtained at some of the node locations, which adversely affected the accuracy of the results.

SUMMARY

Two alternative methods to a traditional bifilar or trifilar pendulum test for obtaining mass inertia properties were discussed in this paper. These alternative methods were used to test a nacelle and hub of a Vestas V27 wind turbine that Sandia National Laboratories had installed. Both methods yielded fairly accurate results.

REFERENCES

1. J. Bretl and P. Conti, "Rigid Body Mass Properties from Test Data," *Proceedings of the 5th International Modal Analysis Conference,* IMAC, London, 1987, pp. 655–659.

2. H. Okuzumi, “Identification of the Rigid Body Characteristics of a Powerplant by Using Experimental Obtained Transfer Functions,” Central Engineering Laboratories, Nissan Motor Co., Ltd., June 1991.

3. W. Leurs, L. Gielen, M. Burghmans, and B. Dierckx, “Calculation of Rigid Body Properties from FRF Data: Practical Implementation and Test Cases,” *Proceedings of the 15th International Modal Analysis Conference*, Tokyo, 1997.

4. N. Okubo, and T. Furukawa, “Measurement of Rigid Body Modes for Dynamic Design,” *Proceedings of the 2nd IMAC*, 1983, pp. 545–549.

5. J. Bretl and P. Conti, "Mount Stiffness and Inertia Properties from Modal Test Data," *Journal of Vibration, Acoustics, Stress and Reliability* 111, No. 2, pp. 134-138, 1989.

6. K. Napolitano and M. Schlosser, “Calculation of Rigid Body Mass Properties of Flexible Structures,” *Proceedings of the 29th IMAC*, Jacksonville, Florida, 2011, pp. 73-94.